Influence of carbonation on the low-temperature consolidation by Spark Plasma Sintering of carbonated calcium phosphate bioceramics

C. Ortali, I. Julien, C. Drouet, E. Champion

Influence of carbonation on the low-temperature consolidation by Spark Plasma Sintering of carbonated calcium phosphate bioceramics

C. Ortali[1], I. Julien[1], C. Drouet[2*], E. Champion[1,*]

[1]Univ. Limoges, CNRS, IRCER, UMR 7315, F-87000 Limoges, France

[2]CIRIMAT, Université de Toulouse, CNRS, INPT, UPS, ENSIACET, 31030 Toulouse, France

***Corresponding authors:**

Eric Champion, PhD

E-mail: eric.champion@unilim.fr Tel: +33 (0)5 87 50 23 63

Full address: IRCER UMR CNRS 7315, Centre Européen de la Céramique,

12 rue Atlantis, 87068 Limoges Cedex, France

Christophe Drouet, PhD

E-mail: christophe.drouet@cirimat.fr Tel : +33 (0)5 34 32 34 11

Full address: CIRIMAT, ENSIACET

4 allée Emile Monso, 31030 Toulouse cedex 4, France

Abstract

Calcium phosphates (CaP) such as biomimetic nanocrystalline apatite or amorphous calcium phosphate are hydrated bioactive compounds particularly suitable for bone repair applications due to their similarity with bone mineral. However, their consolidation in ceramic parts deserves special attention as they are thermodynamically metastable and can decompose into less bioactive phases upon heating. Adapted strategies are needed to obtain bulk bioceramics. Spark Plasma Sintering (SPS) has been shown to allow cold sintering of such compounds at temperatures like 150°C while preserving the hydrated character and nanosized dimensions of the precursor powders. To this date, however, the role of the degree of carbonation of these precursors on the densification of CO_3-bearing CaP compounds via SPS has not been explored despite the natural carbonation of bone. In this work, several carbonated CaP hydrated compounds were prepared and consolidated by SPS and the characteristics of the obtained ceramics was scrutinized with respect to the starting powders. Two carbonation routes were carried out: via volume carbonation during powder synthesis or via subsequent surface ion exchange. All samples tested led to apatitic compounds after SPS, including amorphous CaP. We show that the degree of carbonation negatively affects the densification rate and propose possible hypotheses explaining this behavior. Evolution in the nature of the carbonate sites (apatitic A-, B-types and labile surface carbonates) before and after SPS is also noticed and commented. The consolidation of such compounds is however proven possible, and gives rise to bone-like apatitic compounds with great potential as bioactive resorbable ceramics for bone regeneration.

Keywords: (A) Powders: chemical preparation, (A) Sintering, (D) apatite, (E) Biomedical applications

Declaration of interest: none

1. Introduction

The mineral part of bone is composed of nanocrystals made of a non-stoichiometric calcium phosphate apatite exhibiting a low crystallinity and a chemical composition deriving from that of stoichiometric hydroxyapatite HA: $Ca_{10}(PO_4)_6(OH)_2$. The apatite phase of bone is also poly-substituted by various ions[1],[2]. It contains in particular carbonate ions CO_3^{2-} as main substituting species, with an amount varying typically from about 3 to 8 wt% [2],[3]. Studies have also revealed the existence of less organized ionic environments on the surface of the nanocrystals, known as non-apatitic environments as they do not correspond to the regular apatitic structure[3]–[6]. This layer is significantly hydrated, and the presence of water is thought to explain in part the reactivity of the nanocrystals[7]. These environments are located on the surface of the apatite nanocrystals constituting both the mineral part of the bone[6],[8] and biomimetic synthetic analogs provided that close-to-physiological conditions are used for their preparation. The presence of this surface hydrated ionic layer, combined with the nanometric dimensions of the constituting crystals leading to a large specific surface area, along with plate-like crystal morphology provides a very high reactivity that is used *in vivo* for homeostasis, and can be exploited for developing highly bioactive bone substitutes.

Synthetic carbonated hydroxyapatites and nanocrystalline apatites have been the subject of many studies that aimed to develop new biomaterials for bone substitution [9]–[16]. One of the crucial steps in the development of these ceramic materials is their sintering. Indeed, high temperature causes the destruction of the hydrated surface layer, decarbonation and non-stoichiometric apatite decomposition[17],[18].

In order to consolidate nanocrystalline apatite, previous studies focused on low-temperature sintering by Spark Plasma Sintering[19]–[23]. This flash “cold” sintering

technique, allows to consolidate nanocrystalline apatite powders into porous ceramics typically at 150°C while preserving most of the hydrated non-apatitic environments and the nanosized dimensions of the crystals[21]. In the consolidation process of ceramics at such low temperature, the role of the hydrated layer is thought to be primordial: the ions contained in the hydrated layer being indeed highly labile, ion diffusion through hydrated layers of adjacent nanocrystals can occur even without strong thermal activation[7]. Recently, we investigated consolidation of bone-like carbonated calcium phosphates by SPS at low temperature and showed that the sinterability was greatly enhanced when amorphous carbonated calcium phosphate (ACPs) powders were used in comparison with nanocrystalline ones**[23]**. During SPS, the consolidation occurred at temperatures below 150 °C and it was accompanied by crystallization of the amorphous phase into calcium deficient carbonated apatite $Ca_{10-x-y}(PO_4)_{6-x-y}(HPO_4)_x(CO_3)_y(OH)_{2-x-y-2z}(CO_3)_z$. Using this approach, porous ceramics of non-stoichiometric carbonated apatite, composed of crystalline grains surrounded by a non-apatitic hydrated layer at the grain boundaries and containing 1.5wt% of carbonate were produced, which exhibited an average flexural strength of 18 MPa.

In view of further applications in bone tissue engineering, it is necessary to be able to tune the carbonate amount in the sintered apatite since it may modulate the biological behavior, i.e. biodegradation, osteoclast and osteoblast responses (see references 18 to 27 cited in[14]). In this context, the aim of the present study was to investigate the influence of carbonation amount in carbonated calcium phosphate powders on their consolidation ability by SPS at low temperature. To this end, various powders were synthesized by aqueous precipitation, the carbonation of which was carried out from two distinct routes. On the one hand, a direct carbonation of the whole grains volume was performed during the powder precipitation process. On the other hand, a surface

carbonation of precipitated non-carbonated calcium phosphate powders was performed by surface ionic exchange in solution. Then, low-temperature consolidation was performed by SPS at 150°C. The sinterability, microstructure, chemical structure and composition of the resulting ceramics were analyzed.

2. Materials and Methods

2.1. Carbonated calcium phosphate powders

Amorphous carbonated calcium phosphate powders (Table 1) were synthesized by precipitation in aqueous medium according to the method reported previously[23]. Briefly, a carbonate (NH_4HCO_3, > 99.0%, Sigma Aldrich) and phosphate solution ($(NH_4)_2HPO_4$, 98.7%, Fisher Chemical) was slowly added to calcium nitrate solution ($Ca(NO_3)_2,4H_2O$, 99%, Sigma Aldrich) at constant pH = 9 by addition of an ammonium hydroxide solution ($NH_4(OH)$, Fisher Chemical). The temperature was set to 37°C, the physiological temperature of the human body. Two C/P molar ratios, designating the molar ratio in which the phosphate and carbonate ions were introduced, were investigated: 0.125 and 0.25. The Ca/P molar ratio from the reagent amounts was kept equal to 1.67. The synthesis reactor was put under argon flow. After total addition of reagents, the mixture was left to mature for 30 minutes. Then, the precipitate was filtered, washed with 8 liters of deionized water for about 25g of precipitated powder, and finally lyophilized. The two carbonated powders will be designated as C0125 and C025 corresponding to the 2 ratios C/P = 0.125 and 0.25, respectively.

In order to carbonate only the surface of grains, another carbonation process was investigated by surface ionic exchange. It was performed on three carbonate-free calcium phosphate powders: two calcium deficient hydroxyapatites obtained via two distinct synthesis routes, and an amorphous calcium phosphate.

The first carbonate-free calcium deficient hydroxyapatite compound was prepared according to the same process as that used for the synthesis of carbonated powders but without carbonates. Due to the low synthesis temperature (37°C), non-stoichiometric calcium deficient apatite is obtained [24]. This powder will be referred to as "CDHA" (for calcium deficient hydroxyapatite) in the rest of the manuscript.

The second calcium deficient apatite compound (Table 1) was prepared according to Vandecandelaere *et al.* [25] bio-inspired method, leading to biomimetic apatites. This sample will be referred to as "BNA" (for biomimetic nanocrystalline apatite). The precipitate was formed by the rapid addition of a solution of calcium nitrate to a solution of ammonium hydrogen phosphate at room temperature (22°C). The molar ratio Ca/P of the reactants was set at 0.25, the phosphate ions were therefore present in large excess to maintain the synthesis medium at a pH close to the physiological value (pH = 7.2) thanks to phosphate buffering. The precipitate was then aged for 5 minutes, filtered, washed with 10 liters of deionized water per 25 g of powder and finally lyophilized. The short maturation time of 5 minutes was chosen in order to obtain a powder having a large proportion of hydrated surface layer and therefore a high surface reactivity [26].

A carbonate-free amorphous calcium phosphate (Table 1) was also prepared with regards to the work of Somrani *et al*. [27]. It was obtained at a temperature of 22°C by rapidly pouring 225 ml of calcium solution (0.36 $mol.l^{-1}$) containing 20 ml of NH_4OH 28%, (MERCK) into 750 ml of phosphate solution (0.154 $mol.l^{-1}$) containing 20 ml of NH_4OH 28%. Immediately after the precipitate formation, the mixture was filtered, washed with 1.5 L of deionized water containing 7.5 ml of NH_4OH at 28% and finally lyophilized during 24h. The powder obtained by this method will be named "ACP" (for amorphous calcium phosphate).

The surface carbonation of these three carbonate-free calcium phosphate powders was performed by ionic exchanges in solution. Based on Drouet *et al.* works [28], 2g of free-carbonate powders (CDHA, BNA or ACP) were impregnated in a solution (250 ml) of sodium carbonate ($NaHCO_3$, Carlo Erba Reagent, 99.7%), at a concentration of 0.4 $mol.l^{-1}$ during 12 minutes. Then, the powders were filtered, washed with 1 L of deionized water and lyophilized during 12h. The post-carbonated ACP, BNA and CDHA powders will be named ACP-PC, BNA-PC and CDHA-PC, respectively.

2.2. Spark plasma sintering

Sintering of ceramic pellets was performed using a SPS Dr.Sinter 825 from Fuji Electronic Industrial Company (Japan). It involves application of a uniaxial compressive load on the sample and simultaneous heating by a pulsed continuous electric current. Weighed 300 mg of powder was introduced into a 10 mm diameter graphite die previously covered with Papyex®, a thin graphite foil, to facilitate the demolding of the sample after SPS. Figure A.1 (see supplementary material) gives the SPS temperature and pressure cycles used in this study. The sintering temperature was set at 150 °C with a heating rate of 20 °C min^{-1}. The pressure was set to 80 MPa, applied in 1 min. After application of the compressive stress, a plateau was made at 50 °C during a few minutes to homogenize the temperature in the enclosure of the SPS device. Each test was carried out under argon atmosphere.

The *in situ* densification curves were registered from the measurement of the moving piston displacement and the temperature measured by a thermocouple placed close to the sample inside a hole drilled in the graphite die.

2.3. Samples characterization

X-ray diffraction patterns of as-prepared powders and SPS ceramics were acquired on a BRUKER D8 Advance diffractometer using the CuKα radiation. The patterns were recorded in a 2θ range 20°-60° with a step size of 0.02° and a dwell time of 0.51 sec. Phase identification was performed by comparing the experimental diagram with the database of diffraction patterns (PDF-2, 2004) of the International Center for Diffraction Data (ICDD). Lattice parameters were refined by profile fitting using the JANA2006 software (Czech Republic). Diffraction peaks were fitted according to a pseudo-Voigt function, allowing the system to be anisotropic. The crystallite size L_{hkl} was determined from two peaks ((002) and (310) giving respectively the mean crystallite length and width) by the Scherer equation (eq. 1) [29] and using the Peakoc software (France):

$$L_{hkl} = \frac{\lambda}{cos\,\theta_{hkl}\sqrt{\beta_{exp}^2 - \beta_0^2}} \qquad (eq.1)$$

with λ, the X-ray radiation wavelength; β, the full width at half maximum of the peak (experimental, β_{exp}, or for a reference well crystallized HA compound, β_0) and θ, the diffraction angle of the associated (*hkl*) plane. The lattice distortion parameter g_{hkl} in the crystallographic direction (00*l*) was also calculated based on the model of Hoseman and Vogel (equation 2) [30]:

$$\sqrt{\beta_{exp}^2 - \beta_0^2} = \frac{1}{L_{hkl}} + \pi^2 \frac{g_{hkl}^2}{d_{hkl}} m^2 \qquad (eq.2)$$

with *m* the reflection order and d_{hkl} the reticular distance of (hkl) planes family, applied here to the family of planes (00*l)*.

Fourier-Transform Infrared (FTIR) spectra were collected on a NICOLET 5700 spectrometer. The spectra were recorded in transmission mode, using KBr pellets, over

the 4000 – 400 cm^{-1} range with a resolution of 2 cm^{-1} from an accumulation of 64 scans.

For quantitative chemical analysis, calcium and phosphorus contents were determined by Inductively Coupled Plasma/Optical Emission Spectroscopy (ICP/OES) on a PERKIN ELMER, Optima 8300, Optical Emission Spectrometer. The analysis was performed in solution from about 30 mg of powder dissolved in perchloric acid prepared at 6 $mol.l^{-1}$ (70%, AnalaR NORMAPUR) and diluted in 1000 ml of water. Carbonate content in powders and sintered ceramics was evaluated using FTIR spectroscopy according to Grunenwald *et al.* method [31]. FTIR was also used to estimate the proportions of carbonates within the various location sites (i.e., "A type" substituting hydroxides or "B type" substituting phosphates in the apatite structure, or "labile", corresponding to surface carbonates ions from the hydrated non-crystallized environments).

Particle morphology in the powders and the microstructure of SPS ceramics were observed by scanning electron microscopy (SEM) operating in secondary electron mode (JEOL, FEG-SEM, JSM 7400F). For powders, a few grains were dispersed in acetone and placed on a steel sample holder prior to SEM examination. The pellets observed by SEM were fixed on the sample holder with adhesive carbon tape.

Specific surface area (S_{BET}) of powders was measured by the BET method (MICROMERITICS, ASAP 2020, 8 points). The relative density or densification ratio (τ, %) of SPS ceramic samples was determined by weighing using the Archimedes' method in water and the true density by He pycnometry (MICROMERITICS, AccuPyc II 1340). The densification ratio (τ) was calculated as the ratio of the relative density to the true density.

3. Results

3.1. Powder characterization

The XRD patterns (Figure A.2) of synthetic powders ACP, ACP-PC, C0125 and C025 do not show any diffraction peak. A broad "halo" centered on 2θ = 30 ° is observed, which is characteristic of amorphous calcium phosphates [32], [33]. Conversely, the diffractograms obtained on raw BNA and CDHA powders present the typical diffraction peaks a poorly-crystalline apatite phase (JCPDS 9-432). Post-carbonated powders (BNA-PC and CDHA-PC) exhibit XRD patterns similar to those of their initial carbonate-free counterparts, as would be expected since only surface carbonation has been operated.

The crystallographic parameters of crystallized powders determined from these patterns are reported in Table 2**.** Lattice parameters a and c are similar for all the powders, slightly larger than those of stoichiometric hydroxyapatite (*a* = 9.418 Å and *c* = 6.884 Å – PDF file 9-432). Crystallites are in the nanometric range: about 15 to 18 nm in the (002) direction and 5 nm in the direction (310). The difference along the two directions denotes preferential crystalline growth in the crystallographic *c* direction. In order to evaluate the crystallinity of these powders, the deformation parameter g_{hk1} wass determined in the (00*l*) direction [30]. This parameter is similar for all the powders, about 0.011Å.rad. This parameter is larger than the one determined with stoichiometric HA, synthesized according to Raynaud *et al.* [24], for which g_{hk1} was 0.0030 Å.rad. The difference reflects the very low crystallinity of CDHA, BNA, CDHA-PC and BNA-PC powders, thus closer to natural bone mineral. Finally, there is overall no significant structural change during the post-carbonation of the powders by surface ionic exchange.

SEM micrographs of powders (Figure 1) point out grains of ACP, C0125 and C025 powders of spherical shape, which is typical of amorphous calcium phosphates [34]. The carbonate amount initially introduced during the synthesis was found to affect the grain size and the specific area of powders (Table 3). The average particles size increases from about 35 nm for ACP (C/P = 0) to 125 nm for C025 (C/P = 0.25), and their specific surface area decreases from 67.5 $m^2.g^{-1}$ for the ACP to 37.6 $m^2.g^{-1}$ for the C025 powder. Nevertheless, in the case of ACP, the small grain size and high specific area may also relate to the absence of maturation and the lower synthesis temperature (22°C). CDHA and BNA grains are elongated/needle-like, with a size around 10 to 20 nm in diameter and 30 to 120 nm long for CDHA and around 6 to 15 nm in diameter and 20 to 50 nm long for BNA. These nanometric dimensions agree well with the very high specific surface of these powders (above 200 $m^2.g^{-1}$).

After surface ionic exchange, the post-carbonated powders do not exhibit significant changes in grain size and morphology as illustrated by the example of ACP and ACP-PC (Fig. 1). However, the specific surface area of post-carbonated powders decreases slightly, but the values remain of the same order of magnitude (for example: 178 $m^2.g^{-1}$ for CDHA-PC versus 204 $m^2.g^{-1}$ for CDHA, Table 3). Thus, post-carbonation does not have a significant influence on the morphology of the powders.

FTIR spectra of powders are given in Figure A.3. Amorphous samples (ACP, ACP-PC, C0125 and C025) show broad bands of PO_4 group vibrations at 1040 cm^{-1} (ν_3), 949 cm^{-1} (ν_1), and 560 cm^{-1} (ν_4) [35] and intense bands of H_2O vibrations are detected at 1650 cm^{-1} and in the range 3700-2800 cm^{-1}. Crystallized powders (CDHA, CDHA-PC, BNA and BNA-PC) highlight typical vibration bands of apatitic PO_4 groups at 472 cm^{-1} (ν_2) 560, 575 and 600 cm^{-1} (ν_4), 960 cm^{-1} (ν_1), 1020–1120 cm^{-1} (ν_3). Bands around 632 and 3560 cm^{-1} are assigned to apatitic OH groups [35], [36].

Powders directly carbonated during the synthesis (C0125, and C025) and post-carbonated (ACP-PC, CDHA-PC and BNA-PC) present additional bands attributed to the ν_3 CO_3 (1570-1350 cm^{-1}) and ν_2 CO_3 (900-870 cm^{-1}) vibration modes [35], [37]. Zoom on ν_3 CO_3 vibrations (Figure 2) highlights two broad bands around 1417 cm^{-1} and 1480 cm^{-1}. As there is no obvious contribution for apatitic A-type (at 1540 cm^{-1}) or AB-type (at 1465 cm^{-1}) carbonates in the spectra of crystallized powders (BNA-PC and CDHA-PC) these bands can be assigned to labile carbonates. Accordingly, the broad band centred at 870 cm^{-1} in the ν_2 CO_3 domain (900-850 cm^{-1}) is also attributed to labile carbonates though the wavenumber is slightly shifted to 870 cm^{-1} instead of 866 cm^{-1} as mentioned in previous works[3], [23]. The exact position of the labile carbonate band is indeed still open to investigation as only few insights have been reported so far; also in the co-presence of HPO_4^{2-} ions, a partial superimposition with their 875 cm^{-1} band makes the accurate determination of labile CO_3 band position more complex.

The spectral decomposition of the ν_4 PO_4 domain (500 to 700 cm^{-1}) was carried out, on crystalline powders BNA, BNA-PC, CDHA and CDHA-PC according to the method detailed in previous studies [25], [38],[23], [25]. It allowed following the evolution of the proportion of HPO_4^{2-} ions in apatitic and non-apatitic environments before and after ionic exchanges. Here, apatitic positions refer to the apatitic core of the nanocrystals, and non-apatitic positions refer to surface sites. Relative ratios of integrated intensities of the HPO_4^{2-} bands were calculated. The results are summarized in Figure 3. The proportion of non-apatitic HPO_4^{2-} ions is higher for BNA (0.17) than CDHA (0.11). These non-apatitic HPO_4^{2-} ions are found in an hydrated layer at the apatite nanocrystal surface as described in the literature [13], [37]. Therefore, within the two calcium-deficient apatites produced here, BNA nanocrystals have a larger

hydrated surface layer than those of CDHA. The relative proportion of apatitic HPO_4^{2-} ions (0.06) is similar for these two powders. After ionic exchange, the non-apatitic HPO_4^{2-} ratio decreases in the two powders while their apatitic HPO_4^{2-} ratios remain unchanged by this ionic exchange. Thus, as described by Drouet *et al.*, during ionic exchange, the inserted CO_3^{2-} ions exchange non-apatitic HPO_4^{2-} ions at the surface of the crystals, the apatite core being essentially not modified [28].

Carbonate contents were estimated according to Grunenwald *et al*. method [31]. The results are presented in Table 3. The carbonate content increases with the augmentation of C/P molar ratio of reactants for powders carbonated during the synthesis (C0125 and C025). ACP-PC compound, post-carbonated by ionic exchanges, is the least carbonated powder (1.8 wt% of CO_3^{2-}), which may probably be related to its low surface area (73.9 $m^2.g^{-1}$). The two crystalline powders CDHA-PC and BNA-PC are more carbonated, with respectively 2.1 wt% and 3.8 wt% of CO_3^{2-}. The higher specific surface area of these powders provides a greater exchange surface, which explains the carbonation increase.

The Ca/P ratio of the powders are also given in Table 3. For amorphous powders C0125, ACP and ACP-PC, values of Ca/P molar ratios are less than 1.5, value that corresponds to the theoretical amorphous calcium phosphate composed only of Posner clusters $Ca_9(PO_4)_6$. For C025, the ratio is larger than 1.5., as carbonates are assumed to substitute for phosphates, the Ca/P ratio increases with carbonate substitution. As expected by their synthesis conditions, the crystallized powders (BNA and CDHA) have Ca/P molar ratios smaller than 10/6 (i.e. the value of stoichiometric hydroxyapatite) confirming their calcium-deficiency. After ionic exchange, the global Ca/P molar ratio of post-carbonated powders increases, which is again directly linked

to the decrease of phosphate amount, the non-apatitic HPO_4^{2-} ions being exchanged with CO_3^{2-} ions as stated above.

3.2. Ceramics densification

Densification rates of obtained SPS ceramics are summarized in Table 4. Densification curves (Figure 4) are exploited in the temperature range from 70°C to 160°C, which corresponds to the sample consolidation step. In the temperature range 20-70°C (not shown here), only rearrangement of the powder bed occurs due to the application of the compressive stress.

The behavior of powders initially amorphous differs from that of initially crystallized ones. A fast densification jump at about 130°C (for ACP, ACP-PC and C0125) and 150°C (for C025) followed by a gradual slower densification occurs for amorphous powders while only gradual densification from about 100°C is registered for crystallized compounds (Fig. 4).

Concerning carbonate-free powders (ACP, BNA and CDHA), the final densification ratio is greater for ACP and BNA than for CDHA, with values of 79%, 85% and 68% respectively, showing their greater propensity for cold sintering. The corresponding post-carbonated powders (ACP-PC, BNA-PC and CDHA-PC) show different behaviors with less densification than the initial carbonate-free powders. Carbonated ACP-PC is densified up to 73%, CDHA-PC and BNA-PC powder are only densified at 62%. Moreover, a quasi-absence of densification is observed for CDHA-PC powder (Fig. 4). Thus, surface carbonation obtained by ionic exchanges, causes a decrease of the densification ability of powder compacts during the SPS cycle. This might tentatively be explained by the resulting lower proportion HPO_4^{2-} ions, the proton of which may allow proton hopping between adjacent HPO_4^{2-} species and potentially

favoring densification even at low temperature by increasing locally the electrical conductivity of the sample during SPS.

Densification ratios of SPS ceramics obtained for initially amorphous calcium phosphates (ACP, C0125 and C025) with increasing initial carbonate amounts (0 wt%, 3.1 wt% and 5.9 wt% respectively) decreases from 79% for the ACP to 71% for C0125 and 59% for C025. Therefore, as mentioned above for surface post-carbonation, the bulk carbonation obtained during the direct synthesis of carbonated powders, tends to reduce the densification rate of the ceramic during SPS. Again, this might tentatively be linked to the lower amount of HPO_4^{2-} ions thus limiting proton hopping in the ceramic during sintering, and thus the local electrical conductivity.

3.3. Ceramics characterization

XRD patterns collected on the sintered pellets (Figure A.4) show that ceramics obtained after SPS of initially amorphous powders (ACP, ACP_PC, C0125, C025) exhibit diffraction peaks characteristic of the apatite phase. Thus, SPS induces crystallization of the amorphous compounds prepared here into apatite. The intensity of the diffraction peaks increases and their width decreases when the initial carbonate content of the powder increases (from ACP, ACP-PC to C0125 and C025).

The lattice parameter *a* is around 9.45 Å for all the compositions, which is greater than the value for stoichiometric HA (a = 9.418 Å - PDF 9-431). However, *c* parameter, with values of about 6.88 Å, remains similar to that determined on stoichiometric HA (c = 6.887 Å). Crystallites remain needle-like and exhibit nanometric dimensions (Table 3) from 13 to 36 nm length in the (00*l*) direction and 6 to 14 nm width in the direction (*hk*0). These values (Table 4) highlight that L_{00l} is greater for samples carbonated during the synthesis, 24 nm for ACP and about 36 nm for others initially

amorphous and carbonated compounds. Nevertheless, there is no significant change of the crystallite size during SPS for initially crystallized compounds (BNA, BNA-PC, CDHA_CDHA-PC, Tables 2 and 4). The parameter g_{hk1}, characteristic of lattice deformation, ranges from 0.006 Å.rad to 0.01 Å.rad. It is slightly greater than the value calculated for a very well crystallized stoichiometric HA (0.003 Å.rad). Comparison of the initially crystallized samples before and after SPS (Tables 2 and 4) shows that g_{hkl} decreases, which means that SPS allows increasing sample crystallinity.

SEM micrographs of the ceramics surface (Figure 5) show densified and cohesive materials with intergranular porosity. The grains, whatever their morphology before sintering, i.e. spheres for amorphous powders (ACP, ACP-PC, C012 and C025) or rods for apatitic powders (BNA, BNA-PC-CDHA and CDHA-PC), appear in the form of small rods after SPS. Their size differs according to the nature of the sample. The initially amorphous compounds have the largest grains, measuring between 20 and 50 nm width and between about 45 and 120 nm length after SPS. Ceramics obtained with powders initially crystallized in apatite (CDHA, CDHA-PC, BNA and BNA-PC) have in contrast smaller grains measuring, between 5 and 20 nm in diameter and 20 to 50 nm length. In any case, the anisotropic grains are oriented perpendicular to the direction of the applied pressure during SPS. Post-carbonated samples, more particularly BNA-PC and CDHA-PC, show a greater amount of porosity after SPS, corroborating the low densification ratios of these ceramics (Table 4).

Chemical analysis shows that Ca/P molar ratio of the compounds (Table 4) does not change significantly after SPS but the carbonate content decreases. For the initially amorphous compounds (C0125, C025 and ACP-PC) this decrease is the largest: about 50 wt% of carbonate ions disappears during consolidation by SPS. In the case of initially crystallized compounds, only 25 wt% of carbonates are lost for BNA-PC and

it remains unchanged for CDHA-PC. The carbonate decreases observed can presumably be related to the release of CO_2 gas during SPS. However, this has to be associated to other chemical species to accommodate the remaining O_{2-} ion. One hypothesis could be the reaction between some carbonate ions and adjacent HPO_4^{2-} ions to form CO_2 and H_2O evolved gasses through the reaction:

$2HPO_4^{2-} + CO_3^{2-} \leftrightarrow 2PO_4^{3-} + CO_{2(gas)} + H_2O_{(gas)}$

The infrared spectra (Figure A.5) show the vibrational modes of the phosphate groups (472 cm^{-1} (ν_2) 560, 575 and 600 cm^{-1} (ν_4), 960 cm^{-1} (ν_1), 1020–1120 cm^{-1} (ν_3)) attributed to calcium phosphate apatite, confirming the crystallization of all the materials into an apatite phase [35], [36]. The vibration bands ν_S and ν_L of the hydroxide ions in the apatite structure are also detected at 3560 cm^{-1} and 631 cm^{-1}, respectively. The broad band assigned to water between 3700 and 2800 cm^{-1} decreases after SPS for all the compounds. The ν_2 CO_3 and ν_3 CO_3 vibration domains (Figure 6) show the different types of carbonate ions present in these ceramics. The vibration bands at 878 cm^{-1}, 1465 cm^{-1} and 1542 cm^{-1} confirm the presence of carbonates in the A site of the apatite. The bands at 872 cm^{-1}, 1412 cm^{-1} and 1462 cm^{-1} demonstrates that carbonates are also inserted into the B site of the apatites. Finally, the widening of the bands at 1420 cm^{-1} and the shoulders at 1480 cm^{-1} and 866 cm^{-1} also attest to the presence of labile carbonates after SPS.

Spectral decomposition of FTIR bands in the ν_4 PO_4 and ν_2 CO_3 domains [17], [19] allow to follow the relative proportion of the apatitic and non-apatitic HPO_4^{2-} ions (Figure 7). Apatitic HPO_4^{2-} ions are present in similar amount in all the ceramics. The amount of non-apatitic HPO_4^{2-} is very high in the carbonate-free ACP and BNA ceramics (intensity ratio > 0.20) and drastically lower in the C0125 and C025 compositions (intensity ratio < 0.05). This is coherent with the fact that carbonate ions

are mostly B-type and this occupy the same positions as HPO_4^{2-} in the apatitic core of apatite nanocrystals. For the initially crystallized powders (CDHA, CDHA-PC, BNA, BNA-PC), there is no significant variation of apatitic HPO_4^{2-} during SPS, but the quantity of non-apatitic HPO_4^{2-} increases (Figures 3 and 7). Furthermore, these non-apatitic ions are present in a smaller amount in the ceramics derived from post-carbonated CDHA-PC, BNA-PC and ACP powders than in those resulting from carbonate-free CDHA, BNA and ACP powders. Ceramics sintered from carbonated amorphous C0125 and C025 powders have a much lower amount of non-apatitic HPO_4^{2-} than the other compositions. The increase in HPO_4^{2}- ion content during SPS may be related, as suggested before for SPS-treated non-carbonated apatites [39], to the internal hydrolysis of some PO_4^{3-} ions according to the reaction:

$$PO_4^{3-} + H_2O \leftrightarrow HPO_4^{2-} + OH^-$$

The relative distribution of carbonates in the ceramic after SPS is given in Figure 8. ACP, BNA and CDHA are not considered in this part as they do not contain carbonate. The relative distribution of carbonates appears to be almost the same for all the ceramics: most of them (about 45%) are found as expected in the B sites of the apatite, around 30% are located in the A sites and 20 to 30% of them are labile (surface carbonates within the hydrated layer on the nanocrystals). In the case of BNA-PC and CDHA-PC, already crystallized in apatite before SPS, SPS leads to a majority of the carbonates inserted in the B (52%) or A (31%) sites of the apatite, a smaller amount of them remaining still labile (17%). It must be reminded that for these compositions, the initial carbonte-free powder were post-carbonated by ionic exchange so that carbonate ions were only located in the non-apatitic surface layer of the initial powders' nanocrystals. The position of the carbonates is slightly different in the case of the initially amorphous ACP-PC, where carbonation was also obtained by surface post-

carbonation. Carbonates in B sites are always the most numerous (42%) in the SPS ceramic but only 19% of them are substituted in the A sites and 39% are still labile. The behavior is somewhat similar for the other initially amorphous powders C0125 and C025 that also crystallized during SPS. Labile carbonates, located in the whole volume of the initial grains, are found partly distributed in the A (28 and 25%) and B (44%) sites of the apatite and about 30% of them remain labile.

4. Discussion

Amorphous or crystallized calcium phosphate powders were carbonated in this work by two different routes: in the whole grains volume or only on their surface. A general composition of amorphous calcium phosphates (ACP, C0125, C025) powders carbonated in volume was proposed previously based on Posner cluster formula [23]: $Ca_{9-x-y}(PO_4)_{6-2x-2y}(HPO_4)_{2x}(CO_3)_{2y},nH_2O$ (y = 0 for ACP compound). For these compounds, carbonate and hydrogenphosphate ions are supposed to substitute PO_4^{3-} ions and water is located in the interstices between the clusters. The second carbonation route used here was performed on carbonate-free powders by surface ions exchange, leading to an amorphous powder (ACP-PC) and two crystallized powders (BNA-PC and CDHA-PC) carbonated at their grains surface. This post-carbonation didn't have significant effect on the overall crystallinity and grains morphology. FTIR study also confirmed that CO_3^{2-} was exchanged with non-apatitic HPO_4^{2-} at the grain surface. For these powders, different chemical compositions can be stated. As described above, carbonate-free ACP formula can be approached as $Ca_{9-x}(PO_4)_{6-2x}(HPO_4)_{2x},nH_2O$. After post-carbonation, carbonates are substituted only at the grains surface modifying surface composition of ACP-PC to $Ca_{9-x-y}(PO_4)_{6-2x-2y}(HPO_4)_{2x}(CO_3)_{2y},nH_2O$, the grain core remaining a carbonate-free ACP. Crystallized

apatites (CDHA and BNA) are made of an apatitic core, with more crystal disorder for BNA than CDA, surrounded by a hydrated non-apatitic surface layer. According to the relative proportions of non-apatitic HPO_4^{2-} (Fig. 3) the proportion of surface layer appears more important in BNA than in CDHA. This result also agrees with the synthesis conditions (maturation at 37°C during 30 min for CDHA and only 22°C for 5 min for BNA), the higher the maturation time and temperature are, the less thick is the non-apatitic hydrated surface layer [7]. The crystalline core is a calcium (and hydroxide) deficient apatite which contains apatitic hydrogenphosphate ions (Fig. 3), with chemical formula $Ca_{10-x}(PO_4)_{6-x}(HPO_4)_x(OH)_{2-x}$ leading to Ca/P molar ratios smaller than that of stoichiometric HA (Ca/P = 1.667, Table 3). After ionic exchange, the crystallite composition remains essentially unchanged as only the hydrated non-apatitic surface layer is carbonated.

Carbonation in the whole volume allows to carbonate amorphous powders up to 5.9 wt% whereas ionic exchange in CO_3^{2-} containing medium allows to post-carbonate the powders up to 3.8 wt%, depending on the specific surface area and hydrated surface layer proportions (Table 3). However, for post-carbonated powders it must be noted that the carbonate contents are calculated as average values referring to the total weight of powder grains. So, the real carbonation rate of the grain surface is much higher than these average values.

During SPS, a densification occurs between 120°C and 150°C for all the materials. In any case, carbonated powders are partially decarbonated, probably via a reaction on the grains surface of the type:

$$2HPO_4^{2-} + CO_3^{2-} \leftrightarrow 2PO_4^{3-} + CO_{2(gas)} + H_2O_{(gas)}$$

The presence of non-apatitic (labile) HPO_4^{2-} and CO_3^{2-} ionsin carbonated ceramics, suggests the remaining existence of a non-apatitic hydrated layer on the surface of the apatite nanocrystals even after SPS. Microporous ceramics made of nanoscale rods crystallized in apatite are obtained with a final densification ratio ranging from 59 to 85% depending of the properties of the initial powders.

For initially amorphous powders (ACP, ACP-PC, C0125 and C025), SPS at low temperature results in a faster densification accompanied with crystallization into apatite. For these materials, the same trends are encountered as for initially crystallized powders. ACP-PC and C0125 that have the lowest carbonate amount have the highest densification ratio (73% and 71%, respectively). These ratios are very similar, but ACP-PC ceramic contains only 0.9 wt% of carbonate while it is of 1.5 wt% in C0125 ceramic. So, the initial volume carbonation leads to a better sinterability than surface carbonation of powder grains. A decrease of nearly 50% of CO_3^{2-} amount is registered for the compounds ACP-PC, C0125 and C025, this loss is much lower (no more than 25%) for crystallized powders. Thus, labile carbonates of amorphous powders are more easily removed during SPS than apatitic carbonates of the initially crystallized powders, but a higher proportion of them remains labile after crystallization of the amorphous compound (about 30% vs 17%). As it is the case for initially crystallized powders, the SPS ceramics obtained using amorphous powders contain domains crystallized in apatite and non-apatitic environments.

For initially apatitic crystallized powders (BNA, CDHA, BNA-PC and CDHA-PC), a progressive densification occurs between 100°C and 150°C (Figure 4). The initial powders were weakly crystallized and nanocrystalline. During low temperature SPS, an increase in crystallinity occurs. For post-carbonated powders, a large proportion of initial carbonates remains in the sintered ceramics (with 2.2 and 2.8 wt% for CDHA-

PC and BNA-PC ceramics, respectively). The initial labile carbonates, exchanged for non-apatitic HPO_4^{2-} and located at the grain surface, enter partially into the apatitic crystal core, either in the A (about 30%) or B site (about 50%) and about 17% of them remain labile (Figure 8). This result also explains that BNA and CDHA ceramics present a higher ratio of non-apatitic HPO_4^{2-} species than the BNA-PC and CDHA-PC, part of them being replaced by carbonates in these last ceramics. In any case, the sintered ceramics contain domains crystallized in apatite and non-apatitic environments. The densification ratio of the post-carbonated compounds (τ = 62%) is much lower than those obtained for the carbonate-free compositions (Table 4). Thus, surface carbonation has a detrimental influence on the sinterability. This might be related to the fact that increased (surface) carbonation in turn limits the amount of available HPO_4^{2-} ions and the potential proton hopping among these latter species, which may favor ionic diffusion during SPS. Also, Lafon *et al.* have demonstrated previously that during conventional pressureless sintering of carbonated apatites at high temperature (700-900 °C) under controlled atmosphere (Ar, CO_2/H_2O), carbonation of B site was favorable to the densification of apatites; in contrast, carbonation in A site was unfavorable to the densification [17]. Compared to high-temperature sintering, it can be assumed that the surface carbonates that enter the A sites during the SPS interfere with the densification of the materials and also contribute to reduce their sinterability.

Sintering mechanisms that are active during SPS of these materials differs from natural sintering, and also probably from usual SPS taking into account the low temperatures used here. We showed in a previous work that the combination of an electric field and a compressive stress were mandatory to sinter such ceramics at very low temperature [21]. According to studies on low-temperature SPS [21]–[23] and cold sintering [40],

[41], for these ceramics, migration of species occurs under the combined effect of electrical current and pressure in the presence of hydrated amorphous solid medium (amorphous clusters or surface hydrated layer). This would imply that, in such conditions, surface diffusion is at the origin of the densification phenomenon. Additionally, during this sintering step, chemical reactions involved in the chemical composition modifications, detailed in a previous study [23] occurs. These reactions are summarized in figure 9. Briefly, an internal hydrolysis of non apatitic phosphates PO_4^{3-} may occur [20], leading to the formation of non-apatitic phosphates HPO_4^{2-}. Some of these non-apatitic HPO_4^{2-} ions may however react with labile carbonates, releasing carbon dioxide and forming H_2O and PO_4^{3-} which can be found in the growing nanocrystal (apatitic) or in the hydrated layer (non apatitic). However, since both non-apatitic HPO_4^{2-} ions and CO_3^{2-} ions remain after sintering, these reactions are only partial. The presence of these non-apatitic environments after powder consolidation by SPS implies the remaining presence of a hydrated layer on the surface of apatite nanocrystals in which these environments are located. This means that the ceramics obtained after SPS are composed of a non-stoichiometric carbonate apatite crystalline core constituting the grains, surrounded by a non-apatitic hydrated layer which would constitute the grain boundaries [23].

Finally, Figure 10 summarizes the chemical mechanisms involved during SPS for the three main configurations: crystallized apatite with surface carbonation, amorphous calcium phosphate with surface carbonation and amorphous calcium phosphate carbonated in volume.

5. Conclusion

The carbonation of selected bioactive calcium phosphate powders can be carried out using two different routes: directly in the whole volume during the powder

precipitation or by post-carbonation of carbonate-free powder using surface ionic exchanges. The first route allows to carbonate the compounds up to about 6 wt%. The second one allows for surface carbonation leading to a gobal ratio up to about 4 wt% depending of the specific surface areas of the powder. Chemical modifications occur during SPS, even at low temperature (150°C), which can lead to ceramic materials formed of carbonated apatites. The carbonate ions preferentially locate in the B site of the apatite crystals and a varying proportion remains labile in non-apatitic environments depending of the initial synthesis route. The sinterability is influenced by the carbonate amount. In the same SPS conditions, the densification rate is slightly reduced by increasing the carbonate content, either in the whole volume or in the surface layer of grains.

The consolidated ceramics consist of elongated apatite grains with a preferential orientation in the plane perpendicular to the direction of application of the load. The microstructure consist of crystallized apatite grains whose general formula is $Ca_{10-x-z}(PO_4)_{6-x-z}(HPO_4)_x(CO_3)_z(OH)_{2-x-2y-z}(CO_3)_y$ with $0 \leq x, y \leq 2$ and $0 \leq z \leq 1$ surrounded by a hydrated non-apatitic surface layer allowing to act as a grain boundary and ensure the cohesion of the material. The chemical composition and the crystallinity of the ceramics thus produced are close to those of the mineral part of bones, which would provide improved bioactivity of these biomaterials. Using the various synthesis routes set up, it is possible to tune the carbonate amount (up to 2.8 wt% with the experimental settings of this study) and location into these consolidated “bone-like” ceramics, which should allow the subsequent properties of biodegradability/resorbability to be adjusted. These ceramics are therefore promising for the development of a new generation of consolidated phosphocalcic bioceramics promoting bone regeneration. Among other aspects, this work shows that SPS consolidation of amorphous calcium phosphates allows to produce very poorly-crystallized (therefore expectedly highly reactive) apatitic compounds. This opens the way to the consolidation of ACPs with varying compositions and/or stabilized by use of organic compounds, such as citrate precursors that degrade only from 350°C by heating under air flow[42], provided that the latter remain stable in the low-temperature SPS conditions.

Conflicts of interest

There are no conflicts of interest to declare.

Acknowledgements

C. Ortali thanks to the French “Conseil Régional du Limousin” for her PhD funding and the French Group of the Ceramics (GFC) for financial support of internship at the CIRIMAT Laboratory. This work is supported at IRCER by institutional grants from the LabEX SigmaLim (ANR-10-LABX-0074-01). The authors also thank Sandra Blanchet and Marina Soustre for chemical analyses by ICP-OES and Marion Vandenhende for assistance in SPS experiments at IRCER laboratory.

References

[1] R. Z. LeGeros, "Calcium Phosphate-Based Osteoinductive Materials," *Chem. Rev.*, vol. 108, pp. 4742–4753, 2008.

[2] R. Legros, N. Balmain, and G. Bonel, "Structure and composition of the mineral phase of periosteal bone," *J. Chem. Res. Synop.*, no. 1, pp. 8–9, 1986.

[3] C. Rey, B. Collins, T. Goehl, I. R. Dickson, and M. J. Glimcher, "The carbonate environment in bone mineral: A resolution-enhanced fourier transform infrared spectroscopy study," *Calcif. Tissue Int.*, vol. 45, no. 3, pp. 157–164, May 1989.

[4] A. L. Boskey, N. P. Camacho, R. Mendelsohn, S. B. Doty, and I. Binderman, "FT-IR microscopic mappings of early mineralization in chick limb bud mesenchymal cell cultures," *Calcif. Tissue Int.*, vol. 51, no. 6, pp. 443–448, Dec. 1992.

[5] C. Rey, M. Shimizu, B. Collins, and M. J. Glimcher, "Resolution-enhanced fourier transform infrared spectroscopy study of the environment of phosphate ions in the early deposits of a solid phase of calcium-phosphate in bone and enamel, and their evolution with age. I: Investigations in thev 4 PO4 domain," *Calcif. Tissue Int.*, vol. 46, no. 6, pp. 384–394, Jun. 1990.

[6] D. Eichert, C. Combes, C. Drouet, and C. Rey, "Formation and evolution of hydrated surface layers of apatites," *Key Eng. Mater.*, vol. 284–286, pp. 3–6, 2005.

[7] C. Drouet *et al.*, "Nanocrystalline apatites: The fundamental role of water," *Am. Mineral.*, vol. 103, pp. 550–564, Apr. 2018.

[8] S. Von Euw *et al.*, "Bone mineral: new insights into its chemical composition," *Sci. Rep.*, vol. 9, no. 1, p. 8456, Jun. 2019.

[9] R. Z. LeGeros, O. R. Trautz, E. Klein, and J. P. LeGeros, "Two types of carbonate substitution in the apatite structure," *Experientia*, vol. 25, no. 1, pp. 5–7, Aug. 1968.

[10] G. Bonel, "Contribution à l'étude de la carbonatation des apatites - 1 - Synthèse et étude des propriétés physico-chimiques des apatites carbonatées du type A.," *Ann. Chim.*, vol. 7, pp. 65–88, 1972.

[11] J.-P. Lafon, "Synthèse, stabilité thermique et frittage d'hydroxyapatites carbonatées," PhD Thesis, Université de Limoges, 2004.

[12] S. Cazalbou, C. Combes, D. Eichert, C. Rey, and M. J. Glimcher, "Poorly crystalline apatites: evolution and maturation in vitro and in vivo," *J. Bone Miner. Metab.*, vol. 22, no. 4, pp. 310–317, 2004.

[13] D. Eichert, C. Drouet, H. Sfihi, C. Rey, and C. Combes, "Nanocrystalline Apatite-Based Biomaterials: Synthesis, Processing and Characterization," in *Biomaterials Research Advances*, Nova Science Publishers., 2007.

[14] M.-M. Germaini *et al.*, "Osteoblast and osteoclast responses to A/B type carbonate-substituted hydroxyapatite ceramics for bone regeneration," *Biomed. Mater.*, 2017.

[15] S. Rollin-Martinet, A. Navrotsky, E. Champion, D. Grossin, and C. Drouet, "Thermodynamic basis for evolution of apatite in calcified tissues," *Am. Mineral.*, vol. 98, no. 11–12, pp. 2037–2045, Nov. 2013.

[16] J. C. Merry, I. R. Gibson, S. M. Best, and W. Bonfield, “Synthesis and characterization of carbonate hydroxyapatite,” *J. Mater. Sci. Mater. Med.*, vol. 9, no. 12, pp. 779–783, 1998.

[17] J. P. Lafon, E. Champion, and D. Bernache-Assollant, “Processing of AB-type carbonated hydroxyapatite Ca10−x(PO4)6−x(CO3)x(OH)2−x−2y(CO3)y ceramics with controlled composition,” *J. Eur. Ceram. Soc.*, vol. 28, no. 1, pp. 139–147, 2008.

[18] Y. Doi *et al.*, “Pyrolysis-gas chromatography of carbonate apatites used for sintering,” *J. Biomed. Mater. Res.*, vol. 29, no. 11, pp. 1451–1457, Nov. 1995.

[19] C. Drouet *et al.*, “Bioceramics: Spark Plasma Sintering (SPS) of Calcium Phosphates,” *Adv. Sci. Technol.*, vol. 49, pp. 45–50, 2006.

[20] C. Drouet *et al.*, “Nanocrystalline apatites: From powders to biomaterials,” *Powder Technol.*, vol. 190, no. 1–2, pp. 118–122, Mar. 2009.

[21] D. Grossin *et al.*, “Biomimetic apatite sintered at very low temperature by spark plasma sintering: Physico-chemistry and microstructure aspects,” *Acta Biomater.*, vol. 6, no. 2, pp. 577–585, Feb. 2010.

[22] F. Brouillet *et al.*, “Biomimetic apatite-based composite materials obtained by spark plasma sintering (SPS): physicochemical and mechanical characterizations,” *J. Mater. Sci. Mater. Med.*, vol. 26, no. 8, p. 223, Aug. 2015.

[23] C. Ortali, I. Julien, M. Vandenhende, C. Drouet, and E. Champion, “Consolidation of bone-like apatite bioceramics by spark plasma sintering of amorphous carbonated calcium phosphate at very low temperature,” *J. Eur. Ceram. Soc.*, vol. 38, no. 4, pp. 2098–2109, Apr. 2018.

[24] S. Raynaud, E. Champion, D. Bernache-Assollant, and P. Thomas, “Calcium phosphate apatites with variable Ca/P atomic ratio I. Synthesis, characterisation and thermal stability of powders,” *Biomaterials*, vol. 23, no. 4, pp. 1065–1072, février 2002.

[25] N. Vandecandelaere, C. Rey, and C. Drouet, “Biomimetic apatite-based biomaterials: on the critical impact of synthesis and post-synthesis parameters,” *J. Mater. Sci. Mater. Med.*, vol. 23, no. 11, pp. 2593–2606, Nov. 2012.

[26] N. Vandecandelaere, C. Rey, and C. Drouet, “Biomimetic apatite-based biomaterials: on the critical impact of synthesis and post-synthesis parameters,” *J. Mater. Sci. Mater. Med.*, vol. 23, no. 11, pp. 2593–2606, Nov. 2012.

[27] S. Somrani, M. Banu, M. Jemal, and C. Rey, “Physico-chemical and thermochemical studies of the hydrolytic conversion of amorphous tricalcium phosphate into apatite,” *J. Solid State Chem.*, vol. 178, no. 5, pp. 1337–1348, May 2005.

[28] C. Drouet, M.-T. Carayon, C. Combes, and C. Rey, “Surface enrichment of biomimetic apatites with biologically-active ions Mg2+ and Sr2+: A preamble to the activation of bone repair materials,” *Mater. Sci. Eng. C*, vol. 28, no. 8, pp. 1544–1550, décembre 2008.

[29] P. Scherrer, “Bestimmung der Größe und der inneren Struktur von Kolloidteilchen mittels Röntgenstrahlen,” *Nachrichten Von Ges. Wiss. Zu Gött. Math.-Phys. Kl.*, vol. 1918, pp. 98–100, 1918.

[30] W. Vogel and R. Hosemann, “Evaluation of paracrystalline distortions from line broadening,” *Acta Crystallogr. A*, vol. 26, no. 2, pp. 272–277, Mar. 1970.

[31] A. Grunenwald, C. Keyser, A. M. Sautereau, E. Crubézy, B. Ludes, and C. Drouet, “Revisiting carbonate quantification in apatite (bio)minerals: A validated FTIR methodology,” *J. Archaeol. Sci.*, vol. 49, no. 1, pp. 134–141, 2014.

[32] S. V. Dorozhkin, “Amorphous calcium (ortho)phosphates,” *Acta Biomater.*, vol. 6, no. 12, pp. 4457–4475, Dec. 2010.

[33] A. L. Boskey, “Amorphous Calcium Phosphate: The Contention of Bone,” *J. Dent. Res.*, vol. 76, no. 8, p. 1433–1436., 1997.

[34] A. S. Posner and F. Betts, “Synthetic amorphous calcium phosphate and its relation to bone mineral structure,” *Acc. Chem. Res.*, vol. 8, no. 8, pp. 273–281, Aug. 1975.

[35] C. Rey, C. Combes, C. Drouet, and D. Grossin, “Bioactive ceramics: Physical chemistry,” in *Comprehensive Biomaterials*, vol. 1, 2011, pp. 187–221.

[36] B. O. Fowler, E. C. Moreno, and W. E. Brown, “Infra-red spectra of hydroxyapatite, octacalcium phosphate and pyrolysed octacalcium phosphate,” *Arch. Oral Biol.*, vol. 11, no. 5, pp. 477–492, 1966.

[37] C. Rey, J. Lian, M. Grynpas, F. Shapiro, L. Zylberberg, and M. J. Glimcher, “Non-Apatitic Environments in Bone Mineral: FT-IR Detection, Biological Properties and Changes in Several Disease States,” *Connect. Tissue Res.*, vol. 21, no. 1–4, pp. 267–273, Jan. 1989.

[38] C. Rey, C. Combes, C. Drouet, A. Lebugle, H. Sfihi, and A. Barroug, “Nanocrystalline apatites in biological systems: characterisation, structure and properties,” *Mater. Werkst.*, vol. 38, no. 12, pp. 996–1002, décembre 2007.

[39] S. Rollin-Martinet, “Développement de nouvelles biocéramiques par consolidation à basse température d’apatites nanocristallines bionimétiques,” PhD Thesis, Université de Limoges, 2011.

[40] J. Guo *et al.*, “Cold Sintering: A Paradigm Shift for Processing and Integration of Ceramics,” *Angew. Chem. Int. Ed.*, vol. 55, no. 38, pp. 11457–11461, Sep. 2016.

[41] H. Guo, A. Baker, J. Guo, and C. A. Randall, “Cold Sintering Process: A Novel Technique for Low- Temperature Ceramic Processing of Ferroelectrics,” *J. Am. Ceram. Soc.*, vol. 99, no. 11, pp. 3489–3507, Nov. 2016.

[42] M. Iafisco *et al.*, “Fluoride-doped amorphous calcium phosphate nanoparticles as a promising biomimetic material for dental remineralization,” *Scientific Reports*, vol. 8, art. no. 17016, pp. 1-9, Nov. 2018.

Figure captions

Figure 1. SEM micrographs of initial powders.

Figure 2. FTIR zooms on ν_3 (1570-1350 cm^{-1}) and ν_2 (895-850 cm^{-1}) CO_3 bands of powders (Contributions are denoted A for A-site, B for B-site and L for labile carbonate).

Figure 3. Relative areas of FTIR HPO_4^{2-} bands of crystallized powders before and after ionic exchange.

Figure 4. Densification curves of initially amorphous powders (right) and of initially crystallized powders (left).

Figure 5. SEM of ceramics surface (perpendicular to the direction of the applied load) after SPS.

Figure 6. FTIR zooms on ν_3 (1570-1350 cm^{-1}) and ν_2 (895-850 cm^{-1}) bands of SPS ceramics (Contributions are denoted A for A-site, B for B-site and L for labile carbonate).

Figure 7. Relative areas of FTIR HPO42- bands in SPS ceramics.

Figure 8. ratios of FTIR carbonate bands areas in the ceramics after SPS.

Figure 9. reactional cycle occurring during SPS of carbonated calcium phosphate powders (initially amorphous or containing a non apatitic surface layer).

Figure 10. Schematic representation of different states of carbonated calcium phosphates before and during SPS.

Table captions

Table 1. Table 1: Name preparation conditions and characteristics of the as synthesized powder samples (* The surface of these powders was also post-carbonated by ionic exchange in solutions to produce carbonated samples referred as CDHA-PC, BNA-PC and ACP-PC).

Table 2. Crystallographic parameters of crystallized powders.

Table 3. Specific surface area and compositional features of synthesized powders.

Table 4. Densification ratio, crystallographic properties and chemical composition of SPS ceramics.

Figures

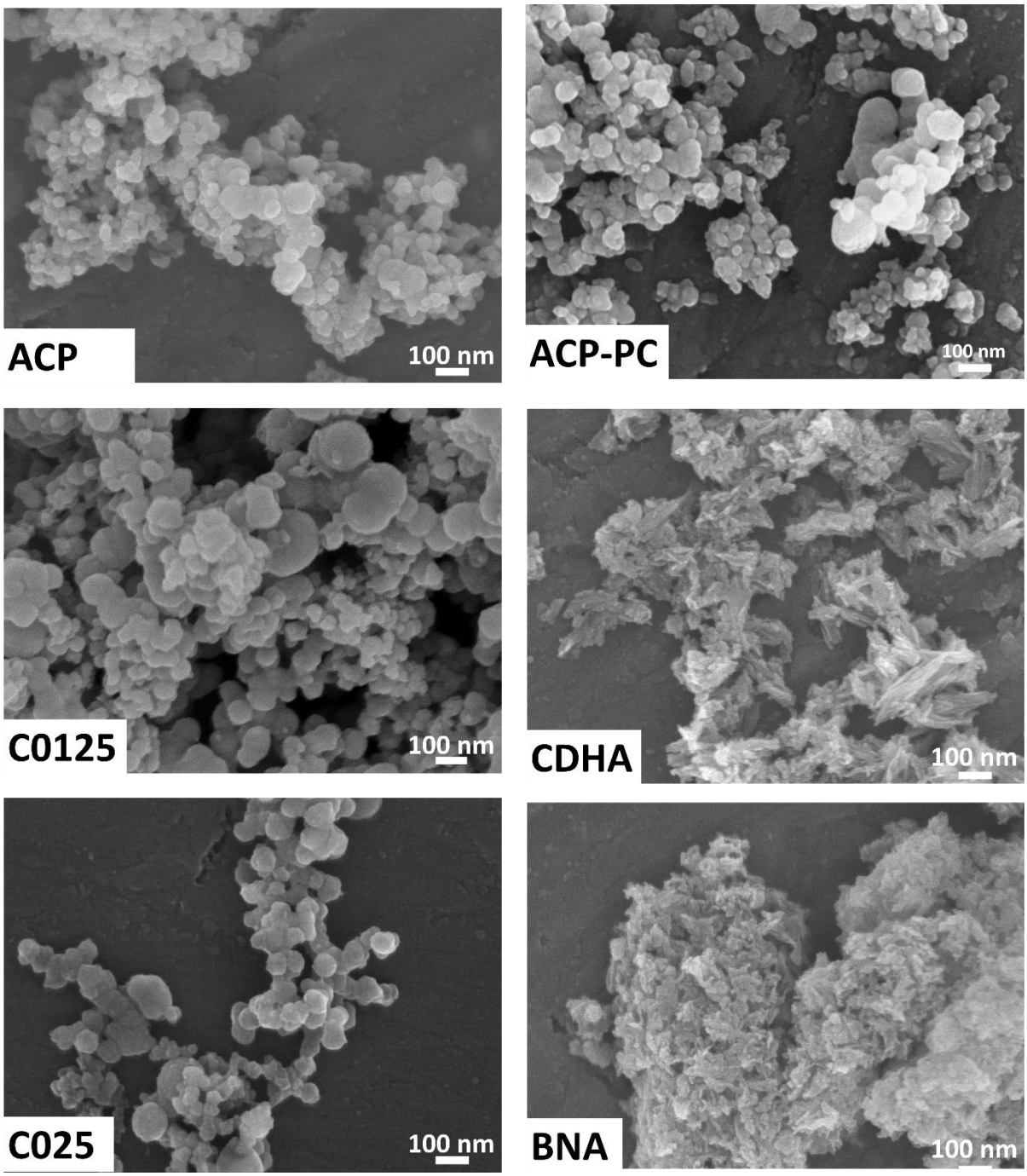

Figure 1: SEM micrographs of initial powders.

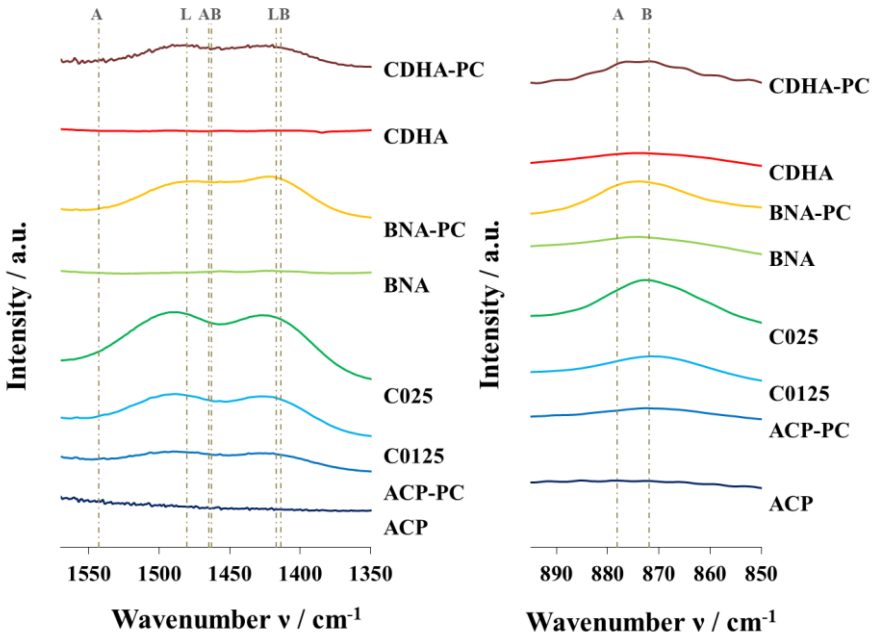

Figure 2: FTIR zooms on ν_3 (1570-1350 cm^{-1}) and ν_2 (895-850 cm^{-1}) CO_3 bands of powders (Contributions are denoted A for A-site, B for B-site and L for labile carbonate).

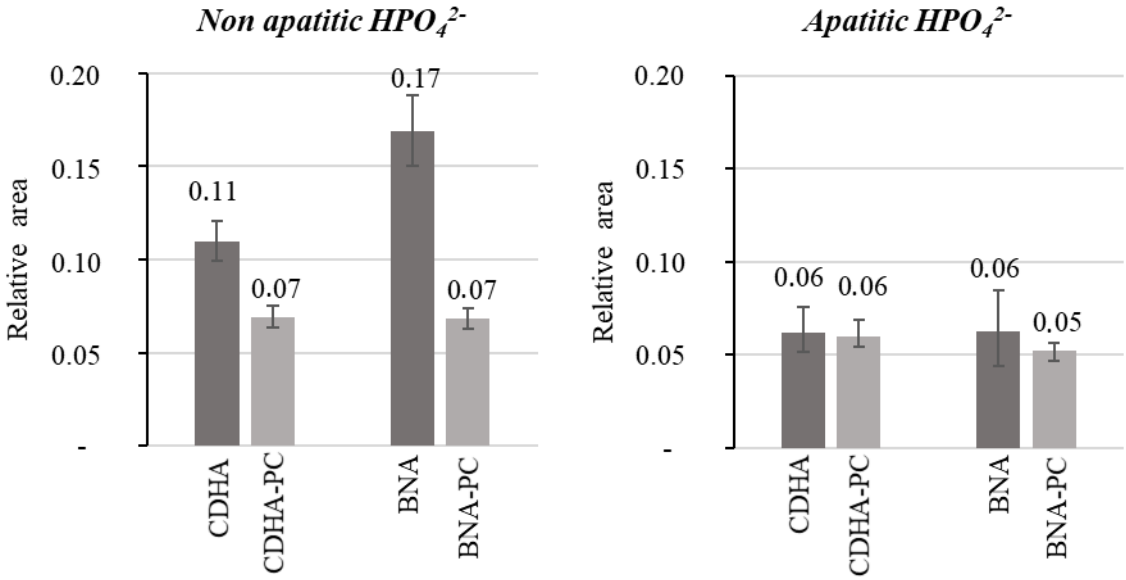

Figure 3: Relative areas of FTIR HPO_4^{2-} bands of crystallized powders before and after ionic exchange.

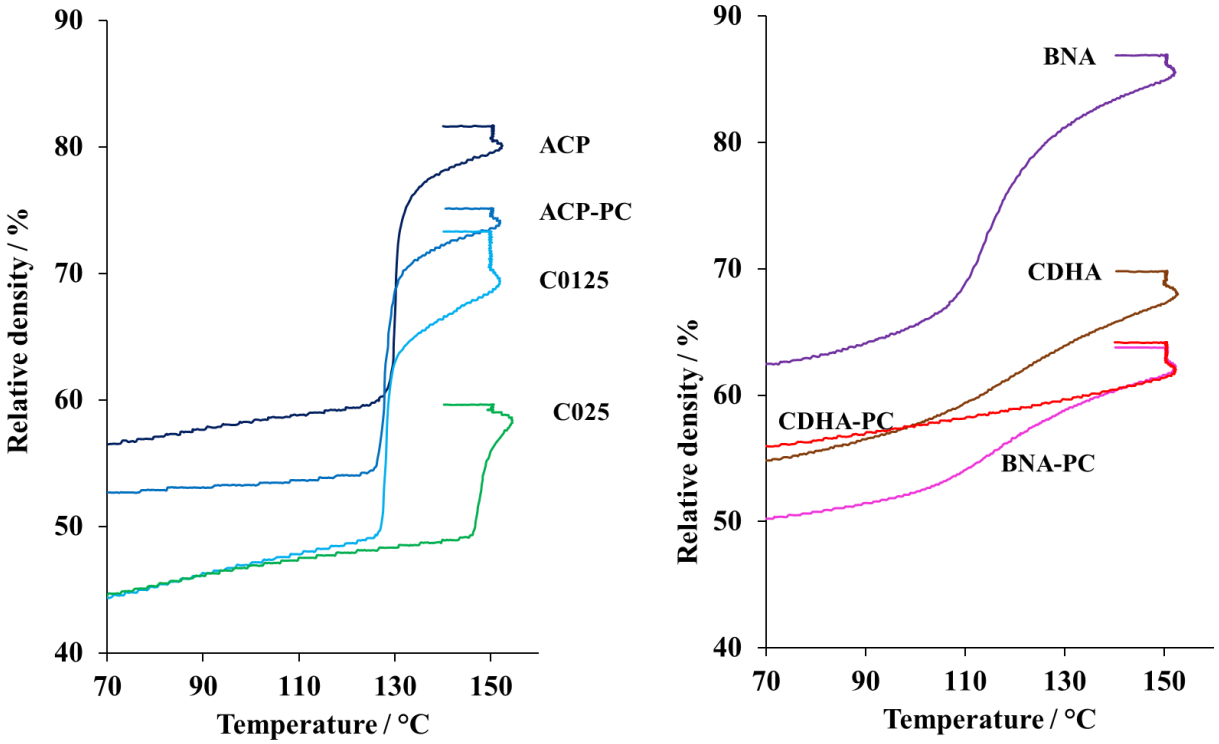

Figure 4: Densification curves of initially amorphous powders (right) and of initially crystallized powders (left).

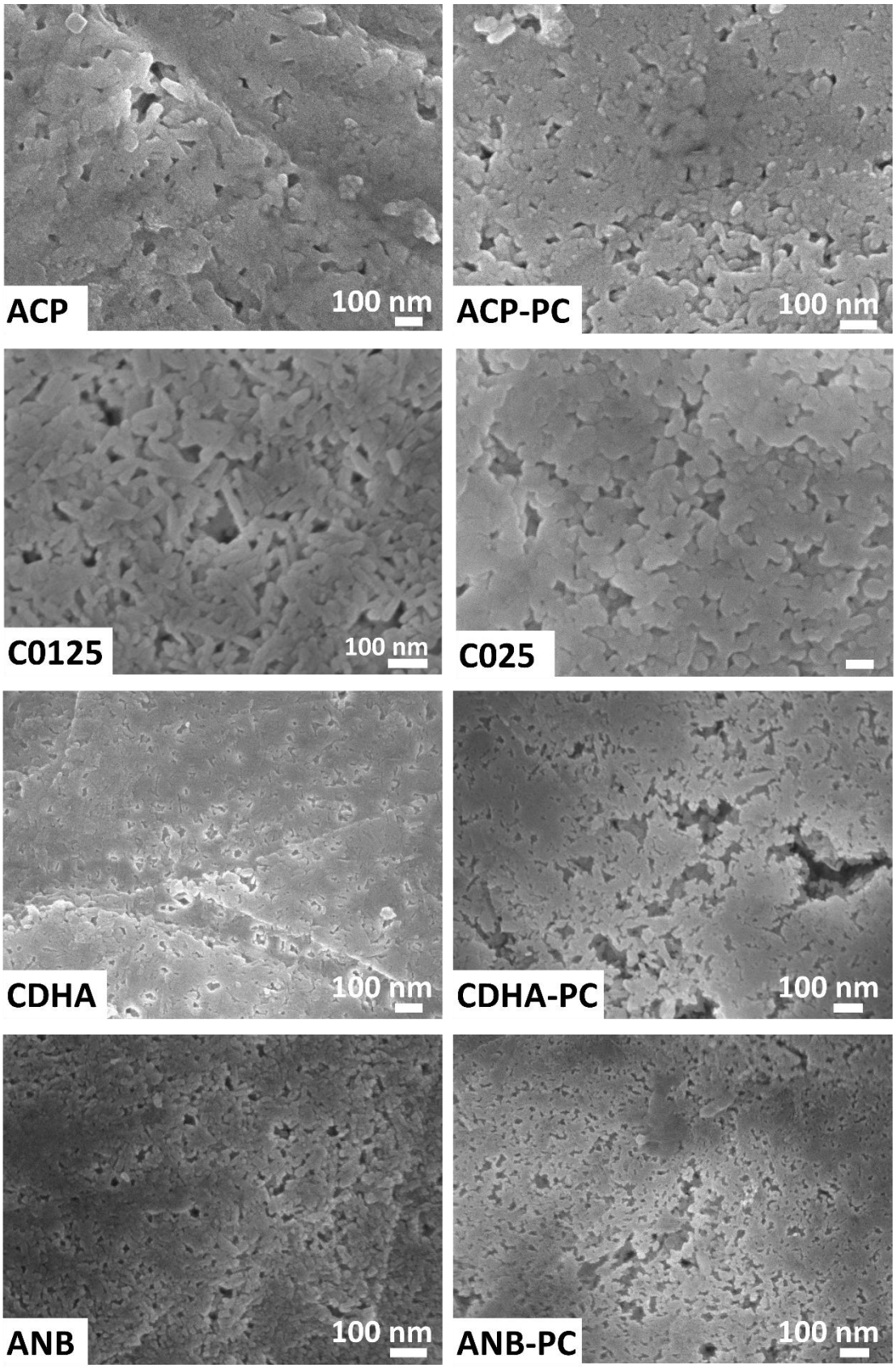

Figure 5: SEM of ceramics surface (perpendicular to the direction of the applied load) after SPS.

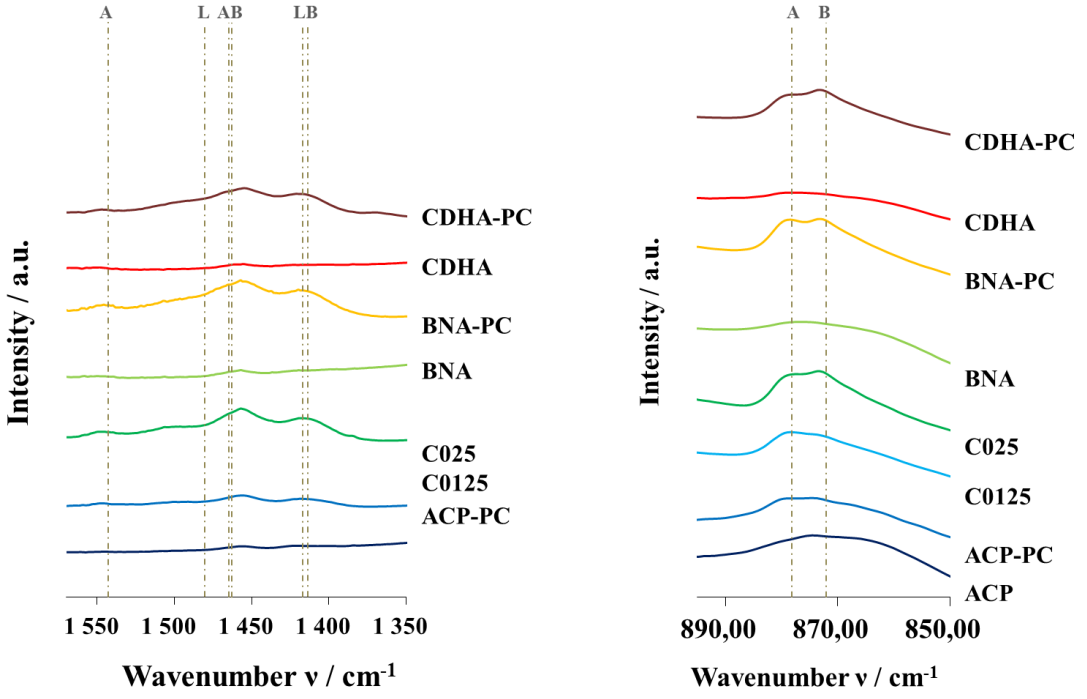

Figure 6: FTIR zooms on ν_3 (1570-1350 cm^{-1}) and ν_2 (895-850 cm^{-1}) bands of SPS ceramics (Contributions are denoted A for A-site, B for B-site and L for labile carbonate).

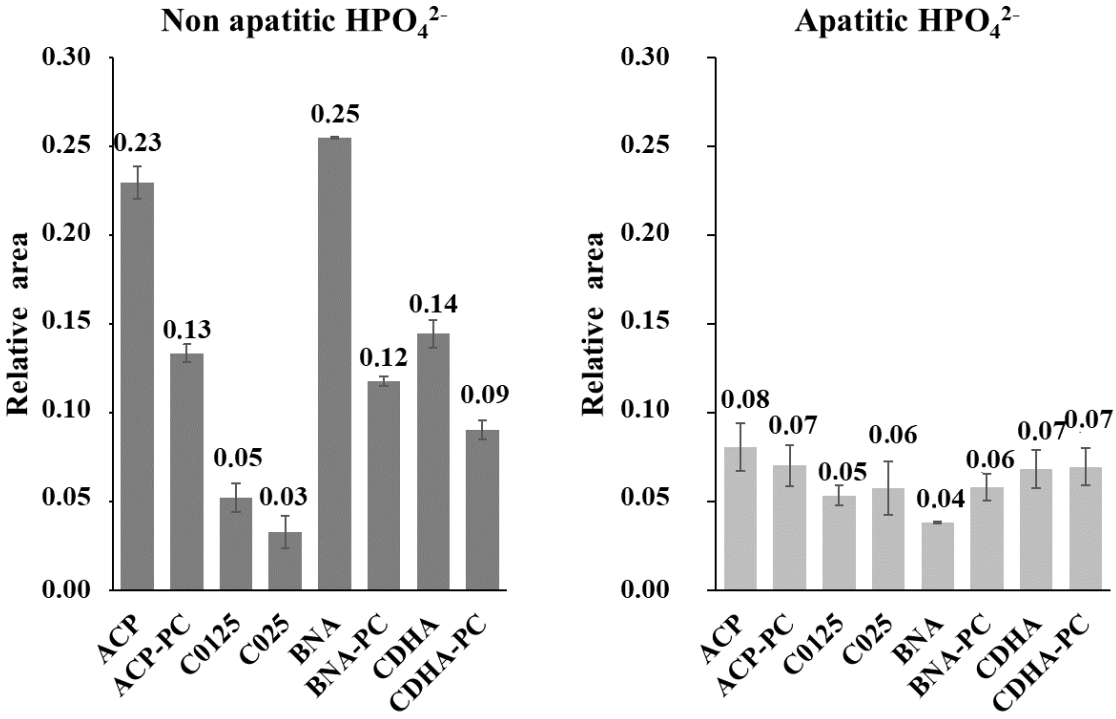

Figure 7: Relative areas of FTIR HPO_4^{2-} bands in SPS ceramics.

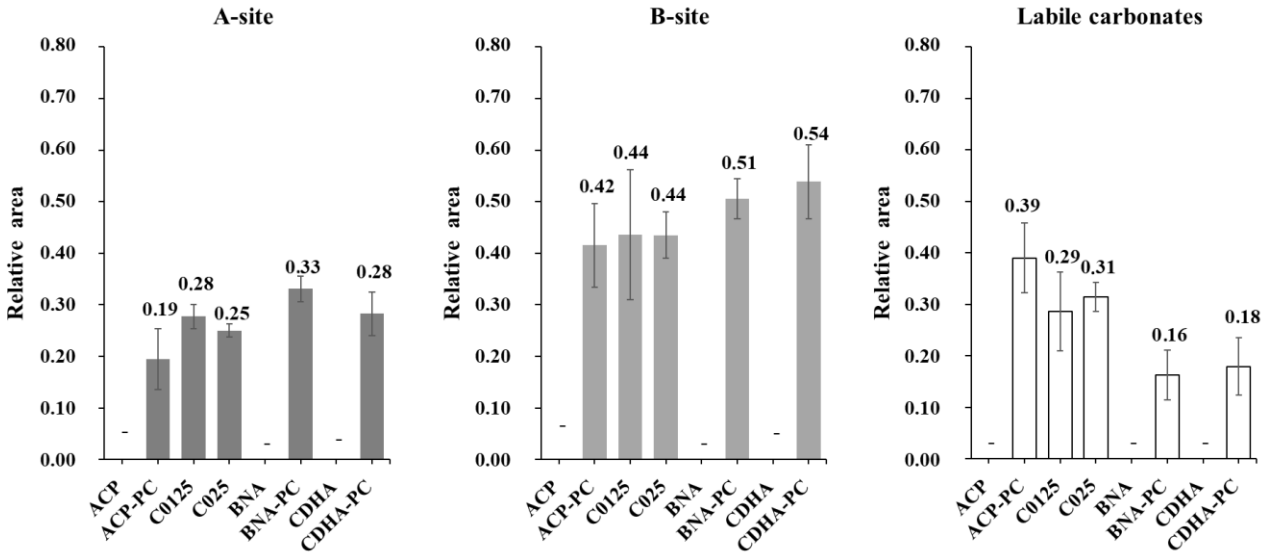

Figure 8: ratios of FTIR carbonate bands areas in the ceramics after SPS.

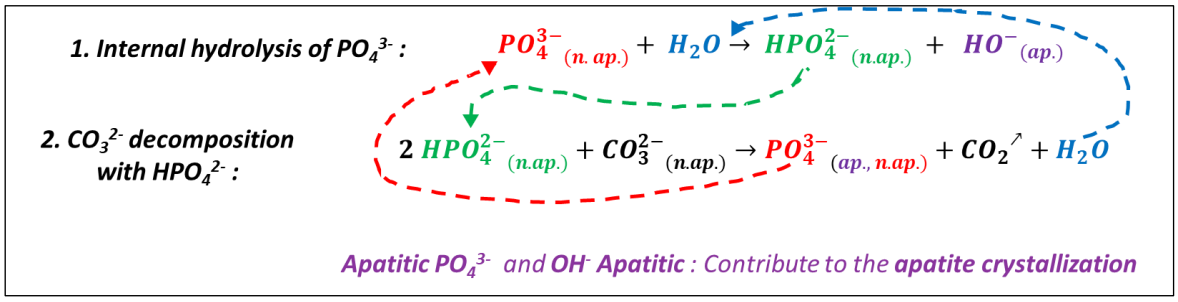

Figure 9: reactional cycle occurring during SPS of carbonated calcium phosphate powders (initially amorphous or containing a non apatitic surface layer).

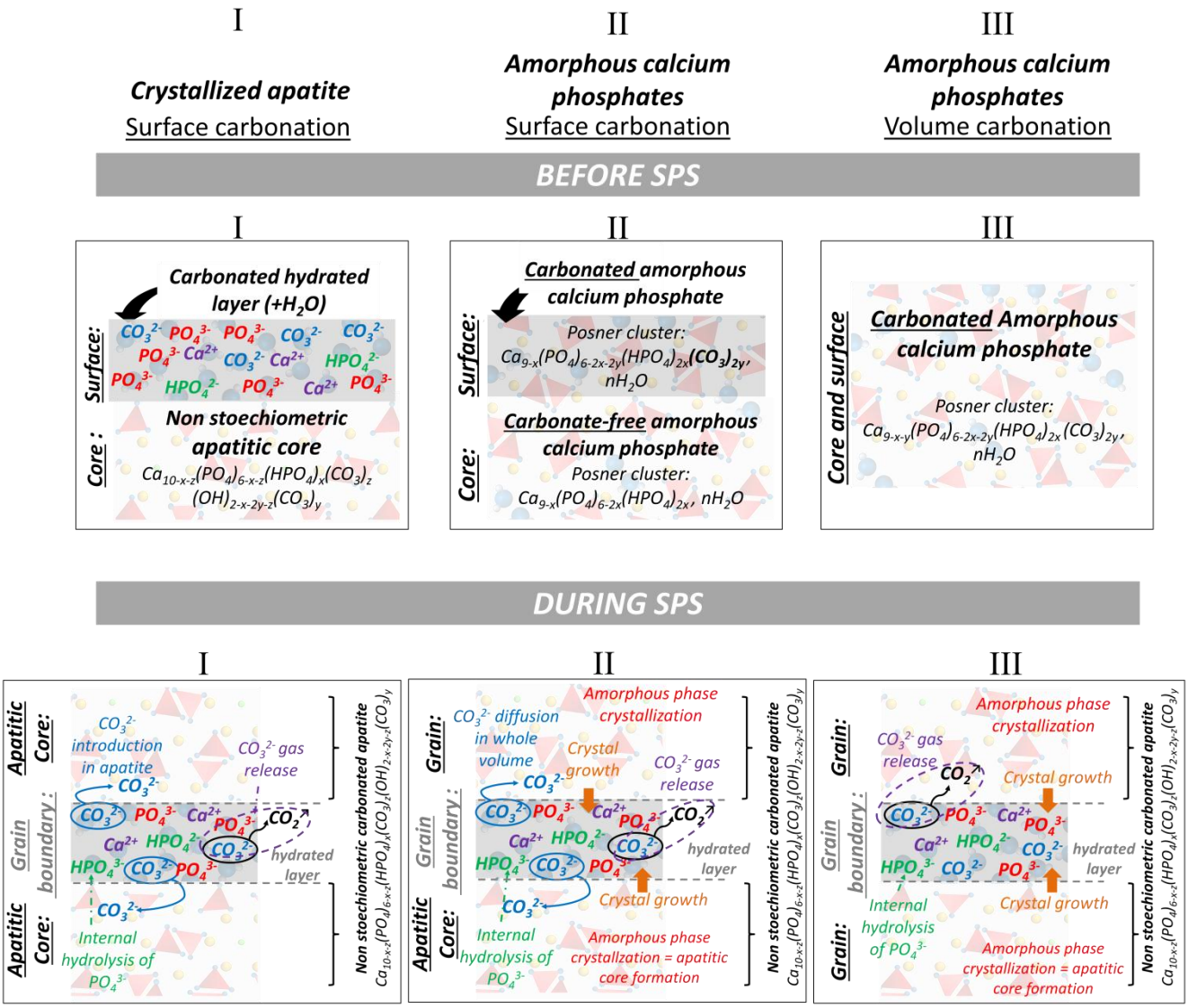

Figure 10: Schematic representation of different states of carbonated calcium phosphates before and during SPS.

Tables

Abbreviation	Synthesis parameters				Characteristics	
	C/P	**Ca/P**	**T (°C)**	**t (min)**	**Structure**	**Grain Morphology**
C0125	0.125	1.67	37	30	Amorphous carbonated calcium phosphate	Rounded
C025	0.25	1.67	37	30	Amorphous carbonated calcium phosphate	Rounded
CDHA*	0	1.67	37	30	Crystallized calcium deficient hydroxyapatite	Needle-like
BNA*	0	0.25	22	5	Crystallized biomimetic nanocrystalline apatite	Needle-like
ACP*	0	0.70	22	0	Amorphous calcium phosphate	Rounded

Table 1: Name preparation conditions and characteristics of the as synthesized powder samples (The surface of these powders was also post-carbonated by ionic exchange in solutions to produce carbonated samples referred as CDHA-PC, BNA-PC and ACP-PC).*

	Initial powder		**Post Carbonated powder**	
	CDHA	**BNA**	**CDHA-PC**	**BNA-PC**
Lattice parameter a (Å)	9.46(2)	9.45(6)	9.45(0)	9.44(9)
Lattice parameter c (Å)	6.88(7)	6.88(8)	6.88(9)	6.89(0)
L_{310} *(nm)*	5 ± 1	5 ± 1	5 ± 1	5 ± 1
L_{002} *(nm)*	17 ± 2	15 ± 2	18 ± 3	16 ± 1
Lattice deformation parameter g_{hkl} *(Å.rad)*	0.0111 ± 0.0008	0.0113 ± 0.0005	0.0116 ± 0.0012	0.0128 ± 0.0003

Table 2: Crystallographic parameters of crystallized powder.

	ACP	ACP-PC	C0125	C025	CDHA	CDHA-PC	BNA	BNA-PC
S_{BET}	67.5±0.5	58.0±0.5	45.8±0.3	37.6±0.3	204.5±0.5	178.9±0.8	260.5±0.7	187.1±0.4
wt% CO_3	0.0	1.8 ± 0.5	3.1 ± 0.5	5.9 ± 0.5	0.0	2.1 ± 0.5	0.0	3.8 ± 0.5
Ca/P	1.29±0.04	1.45±0.03	1.44±0.04	1.64±0.04	1.35±0.06	1.55±0.07	1.33±0.06	1.47±0.07

Table 3: Specific surface area and compositional features of synthesized powders.

Sintered pellet	C0125	C025	ACP	ACP-PC	BNA	BNA-PC	CDHA	CDHA-PC
Densification ratio τ (%)	71 ± 1	59 ± 1	79 ± 1	73 ± 1	85 ± 3	62 ± 3	68 ± 1	62 ± 1
Lattice parameter a (Å)	9.45(7)	9.45(3)	9.44(8)	9.45(2)	9.45(3)	9.44(9)	9.44(9)	9.44(7)
Lattice parameter c (Å)	6.88(7)	6.89(3)	6.87(8)	6.88(3)	6.88(1)	6.88(6)	6.87(8)	6.88(8)
L_{310} (nm)	16 ± 1	23 ± 1	14 ± 1	12 ± 1	7 ± 1	7 ± 1	7 ± 1	6 ± 1
L_{002} (nm)	35 ± 2	38 ± 2	24 ± 3	36 ± 1	18 ± 2	14 ± 2	19 ± 2	13 ± 1
Lattice deformation parameter g_{hkl} (Å.rad)	0.0077 ± 0.0008	0.0064 ± 0.0003	0.0084 ± 0.0003	0.0073 ± 0.0016	0.0082 ± 0.0021	0.0072 ± 0.0010	0.0102 ± 0.0026	0.0096 ± 0.0005
wt% CO_3	1.5 ± 0.5	2.7 ± 0.5	0.0	0.9 ± 0.5	0.0	2.8 ± 0.5	0.0	2.2 ± 0.5
Ca/P	1.42±0.07	1.55±0.07	1.32±0.06	1.42±0.06	1.42±0.06	1.54±0.08	1.36±0.06	1.50±0.07

Table 4: Densification ratio, crystallographic properties and chemical composition of SPS ceramics.